Journal of Petroleum Science and Engineering 203 (2021) 108649

Contents lists available at ScienceDirect

Journal of Petroleum Science and Engineering

journal homepage: http://www.elsevier.com/locate/petrol

Nanomechanical characteristics of trapped oil droplets with nanoparticles: A molecular dynamics simulation

Yuanhao Chang [a], Senbo Xiao [a,**], Yuequn Fu [a], Xiao Wang [b], Zhiliang Zhang [a], Jianying He [a,*]

[a] NTNU Nanomechanical Lab, Department of Structural Engineering, Norwegian University of Science and Technology (NTNU), 7491, Trondheim, Norway
[b] School of Materials Science and Engineering, China University of Petroleum (East China), Qingdao, 266580, Shandong, China

ARTICLE INFO

Keywords:
Nanoparticles
Enhanced oil recovery
Trapped oil droplet
Molecular dynamics simulation
Local pressure distribution
Structural disjoining pressure

ABSTRACT

Nanoparticles (NPs) possess great potentials in applications to enhanced oil recovery (EOR), the underlying mechanisms of which however remain to be explored. In this study, the motion of NPs and the local pressure distribution in a trapped oil droplet/nanofluid system in confined nanochannels are scrutinized by molecular dynamic simulations. Depending on the particle wettability, three different motion patterns have been observed: hydrophilic NPs are more likely to be adsorbed on the solid surface of the channel and stay close to the three-phase contact areas, hydrophobic NPs tend to move inside the oil droplet as clusters, and NPs with mixed hydrophobicity are prone to be trapped at the oil-water interface. It is shown that the existence of NPs introduces high local pressure in the nanochannels, especially at locations where NPs aggregate. Significantly, in the three-phase contact area for hydrophilic NPs, the local pressure distribution features the postulated structural disjoining pressure reported in the literature. For the first time, our molecular dynamics simulation results elucidate nanoparticle-induced structural disjoining pressure at the atomistic scale. The results thus provide a better understanding on the fundamentals of nanofluids in confined channels and serve as guidelines for the design of NPs for EOR applications.

1. Introduction

Oil is indispensable to the world. Till now, more than 50% of the explored oil is still trapped in the reservoir (Lake et al., 2014). The injection of regular chemicals like surfactants or polymers, as the most commonly used agents in enhanced oil recovery (EOR) technology, has approached the limits because of their high cost of makeup for adsorption on the surface and the instability under the harsh reservoir conditions (Abidin et al., 2012; Shah et al., 2010). In contrast, nanoparticles (NPs) have attracted increasing attention because of their characteristics of ultra-small size and significant surface effects. In addition, their relative ease of preparation and good stability in extreme conditions also support their great prospects in EOR in the era of low oil prices (Bera and Belhaj, 2016; Mohanraj and Chen, 2006).

Many experiments have demonstrated the potentials of nanofluids in EOR (Hendraningrat et al., 2013; Hendraningrat and Torsæter, 2016; Hu et al., 2016; Youssif et al., 2018). However, the mechanisms that contribute to the promising results are still under debate despite the previous great efforts (Ravera et al., 2006). Wettability alteration is the most accepted mechanism for NPs in EOR. It's reported that rock surfaces can be changed from oil-wet to water-wet with the insertion of NPs, which leads to the detachment of the residual oil (Al-Anssari et al., 2016; Giraldo, Benjumea, Lopera, Cortés, & Ruiz, 2013; Nazari et al., 2015; Ni et al., 2018). Nevertheless, the mechanism of wettability alteration remains controversial (Dehghan Monfared et al., 2016; Li and Torsæter, 2015; Lim et al., 2015; Ni et al., 2018). Specifically, the wettability alteration in the oil-wet condition was not observed in conventional contact angle test experiments (Nicot et al., 2019). The reduction of interfacial tension is another important mechanism, which has been witnessed in many studies (Rahimi and Adibifard, 2015; Rezk and Allam, 2019; Zhang et al., 2014). Yet, some researchers believe that it hardly contributes to the effect of EOR (Jha et al., 2020; Keykhosravi and Simjoo, 2019; Rostami et al., 2019) and some do not even observe the changes in interfacial tension in their experiments (Dai et al., 2017; Kuang et al., 2018; Metin et al., 2012). In 2003, Wasan and Nikolov postulated the structural disjoining pressure as another mechanism of EOR (Wasan and Nikolov, 2003). They proposed that the NPs can form a wedge-like structure in the three-phase contact area and exert structural

* Corresponding author.
** Corresponding author.
E-mail addresses: senbo.xiao@ntnu.no (S. Xiao), jianying.he@ntnu.no (J. He).

https://doi.org/10.1016/j.petrol.2021.108649
Received 22 January 2021; Received in revised form 5 March 2021; Accepted 7 March 2021
Available online 11 March 2021

disjoining pressure to move forward and detach the oil droplets. Although this theory is supported by static analytical calculation (Chengara et al., 2004; Liu et al., 2012) and was used to explain related nanoparticle aggregation phenomena in experiments (Kondiparty et al., 2012; Matar et al., 2007), the direct quantification of the pressure distribution resulting from structured NPs in the small three-phase contact area has not been reported. Clarification of the dynamic build-up of structural disjoining pressure induced by NPs at the atomistic level is missing. Therefore, there is still ambiguity concerning the intrinsic mechanisms of nanofluids for EOR. Further efforts are needed for elucidating the roles of NPs in the process.

Atomistic modeling and molecular dynamics (MD) simulations are proven to be highly suitable for inspecting the basis of EOR in nanofluid/oil/rock systems (Sedghi et al., 2016; Wu et al., 2015). As a complementary toolset to experiments, MD simulation is very powerful thanks to its accurate controls on the properties of the nanochannels, oil droplets, and NPs, with an atomic resolution. As such, MD simulations were able to uncover the characteristics of the self-assembly of the specific NPs at interfaces and on the droplet (Frost and Dai, 2012; Khedr and Striolo, 2020; Luu, Yu and Striolo, 2013a, 2013b; Sumer and Striolo, 2020). MD simulations were also utilized in investigating oil droplet displacement by nanofluids (Wang et al., 2018a, 2018b, 2019), offering insights into the microscopic transportation mechanism for nanofluids in confined capillaries. So far, atomistic modeling and MD simulations on the nanofluid/oil/rock systems are still sparse, which needs more dedicated inputs in order to obtain a thorough understanding on the fundamentals of nanofluids in EOR and to decipher the large-scale puzzling experimental results.

This study focuses on one of the most important types of residual oil systems, trapped oil droplets surrounded by nanofluids in the throat in reservoirs using MD simulations, aiming to probe the nanomechanical characteristics of the system with different wettability of the NPs. Specifically, the local pressure distribution induced by injection of NPs along the nanochannel is explored, the results of which for the first time provide the atomistic description for NPs migration, nanofluid transportation, and most importantly structural disjoining pressure in the three-phase contact area. This work sheds light on local pressure changes in nanochannels and provides guidelines for predicting the effect of nanofluid injection for screening suitable NPs.

2. Model and simulation details

2.1. Atomistic modeling

The purpose of the modeling is to construct a trapped oil droplet with nanofluid in confined nanochannels. For the sake of simplicity, semi-2D models are chosen in this study to avoid possible curvature tension of the three-phase contact line following previous studies (Rafiee et al., 2012). Different components of the models, as shown in Fig. 1(a), are assembled by ensuring no close atomic contact or overlapping. In total, 4 systems

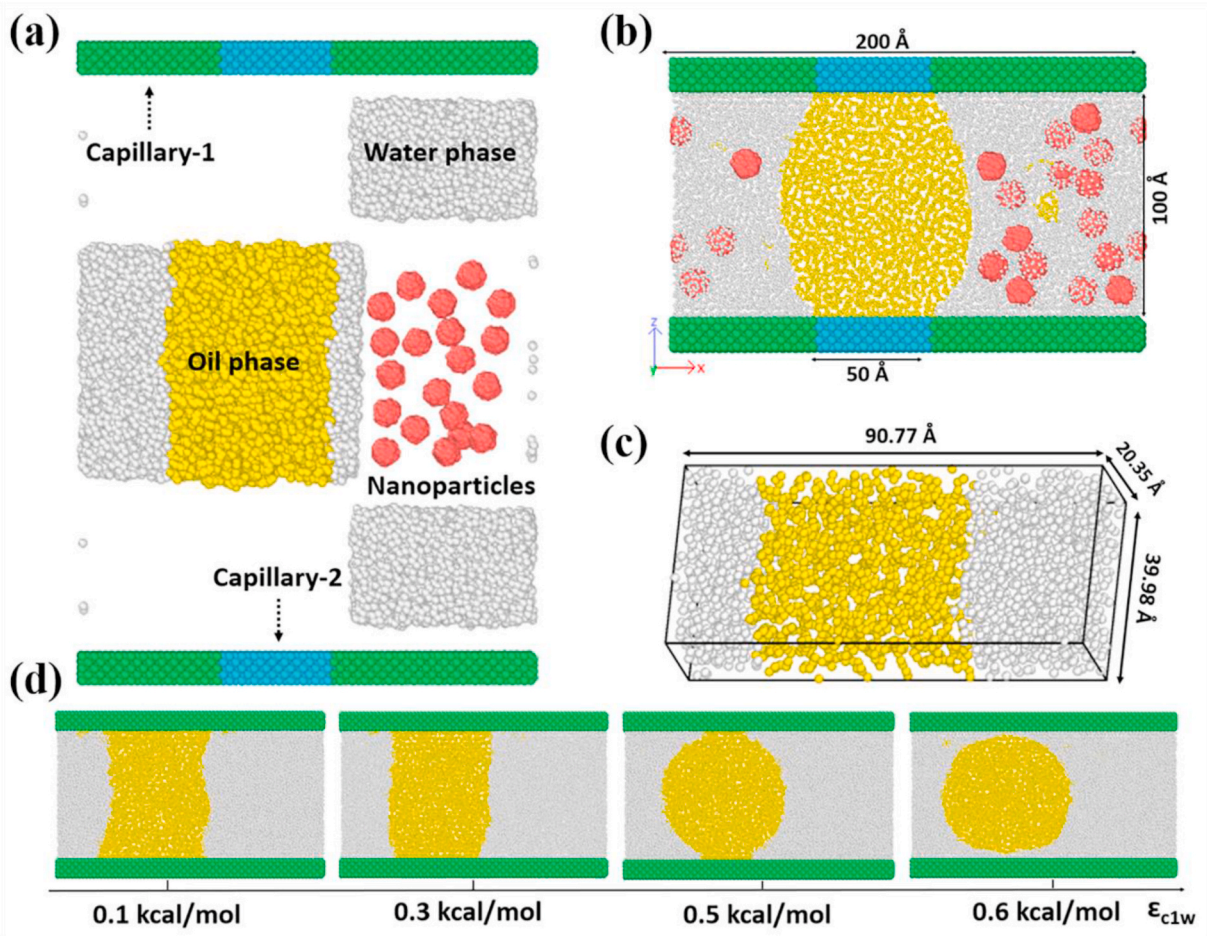

Fig. 1. (a) The side view of an initial system containing oil molecules (yellow), NPs (red), water (white), and solid substrates of an ultra-confined channel (light green and light blue). (b) The side view of a representative equilibrated system. The dimension indicated in the figure applies to all the systems. (c) The extra water/oil system for the calculation of interfacial tension. (d) Oil droplet geometries in nanochannels with varied wettability of the solid substrate. The wettability of the solid substrate is quantified by the LJ energy depth value (ε_{c1w}). (For interpretation of the references to colour in this figure legend, the reader is referred to the Web version of this article.)

are built, namely a base system without NPs, and 3 systems with hydrophilic, hydrophobic, and mixed hydrophobic NPs (termed mix NPs). Each system contains ~25,000 coarse-grained atoms with parameters given in the following text. All the systems are equilibrated for the right water density before data collection and analysis, as the representative equilibrated system snapshot shown in Fig. 1(b) and simulation details given in the following section. The volume of the resulting nanochannel in each system has the same size of $200 \times 25 \times 100$ Å^3, as the dimensions given in Fig. 1(b). It is important to note here that atomistic modeling can only focus on nanoscale sizes that are commonly smaller than experiments.

In order to speed up the simulations, the coarse-grained water model mW and the TraPPE united-atom description of hexane are adopted for water and oil, respectively (Martin and Siepmann, 1998; Molinero and Moore, 2009). Using this coarse-grained model, the resulting oil/water interfacial tension is 52.73 ± 0.98 mN/m (the calculation system can be seen in Fig. 1(c)), in good agreement with experimental data (Leroy, 2016). In all the systems, the final density of the oil and water is controlled according to the experimental values. The nanofluids in the systems contain 20 spherical NPs with a diameter of 10 Å, which corresponds to ~3.3% volume concentration. The NPs and the two solid substrate surfaces share the same diamond cubic crystalline atomic lattice, with a lattice constant of 5.43 Å. The thickness of the two substrates is 11 Å, larger than the non-bonded interaction cutoff distance of 10 Å. All the NPs are treated as rigid bodies for maintaining their spherical geometry. The two substrates are fixed in the equilibration simulations. In order to maintain the oil droplets at their positions in the nanochannel to obtain stable internal pressure profiles, both the upper and lower substrates are composed of two kinds of atom types, namely hydrophobic atoms (in light blue, termed capillary-1) for anchoring the oil droplet and the hydrophilic atoms (in light green, termed capillary-2). The width of hydrophobic regions in the nanochannel is adopted to be greater than the cut-off distance to avoid the possible interactions between fluids on the two sides of the oil droplet, and large enough for localizing the oil droplets in stable positions. The hydrophobic atoms on the solid wall are covered by the oil droplets of different contact angles in this study. It is important to note that there is a distribution of oil-like regions on the wall of the nanochannels in rock due to the long-term oil contact environment and clay minerals in reservoirs, which can stably localize oil droplets. The design of the surfaces thus corresponds to wettability characteristics of nanochannels with trapped oil droplets in an actual reservoir.

The mW model interacts with each other following the Stillinger−Weber interaction potential:

$$E = \sum_i \sum_{j>i} \phi_2(r_{ij}) + \sum_i \sum_{j\neq i} \sum_{k>j} \phi_3(r_{ij}, r_{ik}, \theta_{ijk}) \quad (1)$$

$$\phi_2(r_{ij}) = 7.049556277\varepsilon[0.602245584(\frac{\sigma}{r_{ij}})^4 - 1]exp(\frac{\sigma}{r_{ij} - 1.8\sigma}) \quad (2)$$

$$\phi_3(r_{ij}, r_{ik}, \theta_{ijk}) = 1.2\varepsilon[cos\theta - cos109.47^\circ]^2 exp(\frac{1.2\sigma}{r_{ij} - 1.8\sigma})exp(\frac{1.2\sigma}{r_{ik} - 1.8\sigma}) \quad (3)$$

where van der Waals radius $\sigma = 2.3925$ Å and energy well depth $\varepsilon_{ww} = 6.189\ kcal/mol$. There is an angle-dependent energy term (θ) in the potential, catching the properties of hydrogen bonding in water. The TraPPE-United Atom force field parameters are applied to the interactions of the oil molecules. The pairwise non-bonded interactions for oil-oil and oil-water follow the Lennard-Jones (LJ) potential:

$$U_{LJ} = 4\varepsilon_{ij}[(\frac{\sigma_{ij}}{r_{ij}})^{12} - (\frac{\sigma_{ij}}{r_{ij}})^6] \quad (4)$$

with energy well depths for oil-oil and oil-water as $\varepsilon_{oo} = 0.091411522\ kcal/mol$ and $\varepsilon_{ow} = 0.119147846 kcal/mol$, respectively (Martin and Siepmann, 1998). The interactions between the solid substrate and the liquid are also described by the LJ potential. Specifically, atoms of the hydrophobic capillary (capillary-2) have the same LJ parameters as the oil molecules, while atoms of the hydrophilic capillary (capillary-1) interact with oil having the same energy depth as ε_{ow} (namely $\varepsilon_{c1o} = 0.119147846\ kcal/mol$). In order to feature the appropriate hydrophilicity (water-wet), the interaction energy depth between the atoms of capillary-1 and water was set to be $\varepsilon_{c1w} = 0.6\ kcal/mol$, as testing simulations for water wetting parameters shown in Fig. 1(d). The interaction energy depths between NPs with water (ε_{nw}), oil (ε_{no}) and the solid substrate are given in Table 1. Except for water atoms, all the atoms in the system have the same LJ radius of the CH_2 group defined by the TraPPE united-atom force-field (Martin and Siepmann, 1998). Atoms in the systems are free of charge.

2.2. Simulation details

Three subsequent simulations are carried out on individual systems using the LAMMPS package (Plimpton, 1993). First, the solid substrates (the upper and lower capillaries) in the initial system (Fig. 1(a)) are moved together to reach the right density of the water and oil phases, allowing the atoms in the liquid phase to adjust their positions. Second, energy minimization is performed on the resulting systems with the right fluid density. Third, equilibration simulations are then carried out with all the systems in the NVT ensemble. The systems are kept at 300 K using the Nosé–Hoover thermostat with a damping coefficient of 100 fs (Hoover, 1985; Nosé, 1984). In order to maintain the initial stability, the equilibrations are carried out for 1 ns with a small-time step of 1 fs, and afterward another 200 ns with a bigger time step of 5 fs. Because of the phase separation, the geometry of the three-phase contact area, and the distribution of NPs in the systems are stabilized in the second half of the simulation. The analysis is then focused on the results of the last 100 ns of the equilibration simulations. In order to obtain a more detailed pressure distribution, the system is divided into bins with a length of 2 Å along the nanochannel. The local pressure distribution along the nanochannel is monitored by using the "stress/atom" compute function to sum up the stress per atom in the corresponding region, and which is then normalized by the volume of the bin. The calculation followed the Harasima method in previous studies (Sonne et al., 2005; Yesudasan, 2019). The general pressure expression of per-atom stress can be seen below (Atomic and Simulator, 2003; Plimpton et al., 2007):

$$S_{ab} = -mv_a v_b - W_{ab} \quad (5)$$

with the first term accounts for kinetic energy contribution and the second term for viral contribution. The subscript a and b in the equation denote values of x, y and z components of the quantities. The internal interactions in each NP are neglected since NP is considered as the single rigid in the simulation. The local pressure profiles along the nanochannel are monitored around 5 independent simulation time points in the second half of the equilibration simulations for featuring the ensemble average of the systems. Specifically, time windows of 50 ps at each time point are used for calculating the average local pressure in the nanochannel. The further average of the 5 independent local pressure data set is taken as the local pressure profile of each system. To further

Table 1
Characteristic energy between different NPs with water, oil, capillary-1, capillary-2.

Characteristic energy, kcal/mol	Water	Oil	Capillary-1	Capillary-2
Hydrophilic NPs	0.6	0.119147846	0.6	0.119147846
Mixed NPs	0.119147846	0.119147846	0.119147846	0.119147846
Hydrophobic NPs	0.119147846	0.6	0.119147846	0.6

confirming the significance of the local pressure profiles, time windows of 5 ns are also used to calculate the local pressure profiles. Differences in pressure profiles between systems with and without NPs can be considered as local pressure induced by the existence/injection of NPs.

3. Result and discussion

3.1. Characteristics of the fluid inside the nanochannel

3.1.1. Equilibration of the nanofluids

The aim of the equilibration simulations is to prepare stable systems for revealing phenomena induced by the injection of different NPs. As the initial systems are assembled by different components, it is important to allow these components in the system to relax and unfold any possible unfavorite packing. Especially, the NPs need a certain time to diffuse in the nanochannels for an equilibrium distribution. Thanks to the coarse-grained nature of the water model and the united-atom oil molecules as well as the resulting fast molecular dynamics (Martin and Siepmann, 1998; Molinero and Moore, 2009), the systems reach their equilibrium rapidly. As shown in Fig. 2(a), the total potential energy and temperature of the systems reach plateau values in the first 50 ns of the simulation and maintain the states to the end of the 200 ns equilibration. As mentioned in the Methods section, it is desired to model the correct density of the oil and water phases in all the systems. As such, internal local pressure variations can be directly attributed to the injection of the NPs in the nanochannels. As shown in Fig. 2(b), the density profiles of oil and water along the nanochannels in equilibrium indeed have the appropriate values. The oil droplets in all the systems are positioned stably at the designated places in nanochannel without drifting along the channels, which guarantees a simplified comparison of pressure distribution as detailed in the following discussion.

The NPs in this study are specifically designed to feature different distribution patterns and thus trigger changes in local pressure in the nanochannels for comparison with the base system without NPs. As system snapshots in the course of the equilibration simulations shown in Fig. 2(c), the NPs indeed diffuse in different manners and favor distinct positions in the channel in equilibrium. The hydrophilic NPs migrate only in the water phase during the whole simulation and seem to prefer

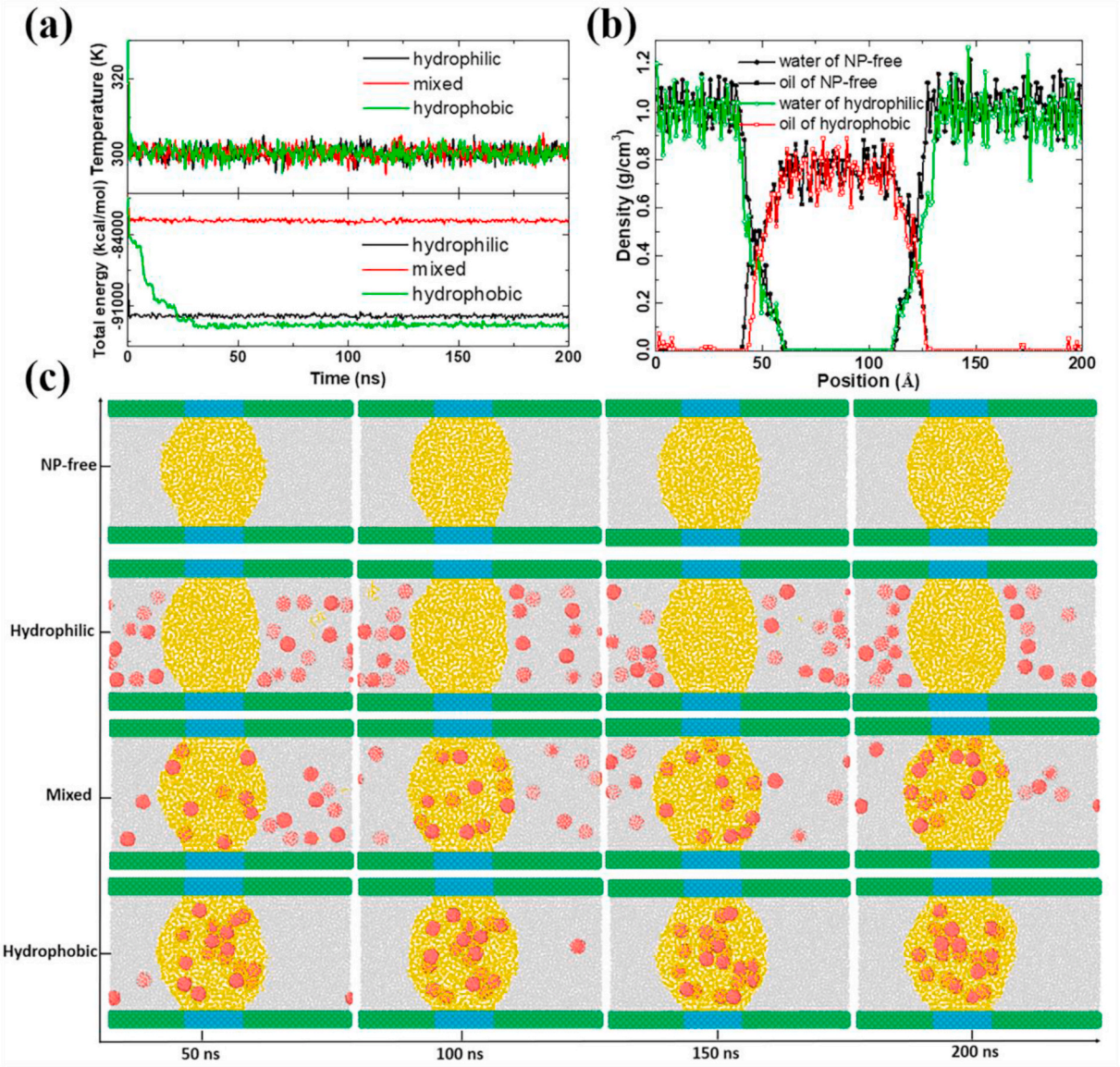

Fig. 2. (a) System potential and temperature in equilibration simulations. (b) Density profiles of the oil and water phases in the base system, the oil phase in the system with hydrophilic NPs, and the water phase in the system with hydrophobic NPs in equilibrium. (c) Snapshots of the 4 systems in the equilibration process. Here, the x-axis represents the simulation time while the y-axis notes the wettability of NPs.

staying close to the oil-water interface and the three-phase contact area. In contrast, most of the hydrophobic NPs move into the oil droplet in the first half of the equilibration simulation. After 100 ns, all the hydrophobic NPs are inside the oil droplet, leading to an obvious expansion of the volume of the oil phase. Because the oil droplet in the system is pinpointed by the hydrophobic capillary-1 area, the contact angle of the oil phase is enlarged with the intake of the hydrophobic NPs. It is reasonable to speculate that the enlarging contact angle of the oil phase by hydrophobic NPs could have a significant impact on the displacement of the oil droplet. Both the dynamics of hydrophilic and hydrophobic NPs in equilibrium are similar to the results monitored in previous studies (X. Wang et al., 2018a, 2018b). The mixed NPs distribute both in water and oil at the end of the equilibration simulation. The partial intake of the mixed NPs in the oil phase also has the effect of enlarging the contact angle of the oil phase. The base system has a stable trapped oil droplet in the whole equilibration and serves as a reference for comparison.

3.1.2. Flow characteristics of the fluid

As shown in Fig. 2(c), there are five kinds of motion behaviors observed in the simulation: NPs disperse in the water phase, NPs disperse in the oil phase, NPs adsorb at the interface (defined by atomistic contact with both the oil and water phases), NPs adsorb on the capillary (defined by stable contact with the first structure water layer at the water-solid interface), and NPs clustering (defined by direct contact between NPs). The number of each behavior is recorded in Table 2. After 100 ns, the trend of motions becomes highly stable. Besides the obvious phenomena that hydrophilic NPs only stay in the water while hydrophobic NPs appear in oil, the hydrophilic NPs are prone to adsorb on the capillary and the hydrophobic NPs in the oil phase can form clusters. The mixed NPs not only disperse in oil and water but also can be trapped at the oil-water interface.

3.1.3. Effect of NPs on the thickness of the oil-water interface

The interfacial thickness between the oil and water phase is one of the crucial properties in determining oil displacement, which also has a strong relationship with the contact angle and the interfacial tension (Xiao Wang et al., 2018a, 2018b). The oil-water interfacial thickness was quantified following the so-called “90-90” criterion (Xu et al., 2013). As illustrated in Fig. 4(a), for each side of the interface, the interfacial thickness is the distance between the positions where the density of oil or water reaches 90% of bulk density. The changes in the total interfacial thickness for the 4 systems are monitored and shown in Fig. 4(b). Approximately, the interfacial thickness in the systems can be divided into two stages: a first developing stage and an equilibrium stage. At the developing stages, the NPs are moving to seek stable dwelling locations. As many of the hydrophobic and mixed NPs migrate into the oil droplet, the interfacial thickness of the systems increases correspondingly. Because the hydrophobic NPs favor the oil phase most, all the hydrophobic NPs accumulate in the oil phase in equilibrium (100–200 ns), resulting in the largest interfacial thickness among the 4 systems. Although quite a number of mixed NPs also enter the oil phase in equilibrium, the change in the resulting interfacial thickness is less obvious. Interestingly, the interfacial thickness with surrounding hydrophilic NPs is slightly larger than in the base system with NPs, despite all the hydrophilic NPs are in the water phase. The results thus indicate injection of NPs can thicken the oil-water interface.

In general, the smaller the interfacial thickness, the higher interfacial tension (Douillard, 2009). The interfacial tension at the oil-water interface alters with the appearance of the NPs in equilibrium. Among the systems, the hydrophobic NPs lead to the largest reduction in interfacial tension. The mixed NPs have a more significant impact on the interfacial tension than the hydrophilic ones. It seems that the volume expansion of the oil phase by intaking NPs is the main driving force for thickening the oil-water interface. Even though many hydrophilic NPs dwell close to the oil-water interface and some are even trapped in the three-phase contact region, their effect on changing the interfacial thickness is not obvious. Although the interactions between hydrophilic NPs with the oil phase are stronger than the counterparts of oil-oil interaction (LJ energy depths are given in the Methods section and in Table 2), the contribution of non-bonded interactions in altering interfacial thickness is not significant.

3.2. Local pressure analysis

3.2.1. Local pressure distribution along the nanochannels

As the positions of most of the NPs in the nanochannels are stable in the second half of the equilibration, systems snapshots in time windows close to simulation time points of 120 ns, 140 ns, 160 ns, 180 ns, and 200 ns are taken as the independent sampling windows for evaluation of the local pressure distribution in the nanochannels. The value of the calculated local pressure reflects the magnitude of the interaction force between atoms in the corresponding region. The local pressure in the 3 systems with NPs is normalized by the average local pressure in the base system without NPs, which are shown in Fig. 5(a). Despite the small sizes, the surface of an NP is a solid surface to individual water and oil molecules, which impose local surface tension in the nanofluid systems.

Table 2
The amount NPs in each system exhibiting the five micro-behaviors stably monitored in the equilibration simulation.

Time(ns)	Hydrophilic				Mixed				Hydrophobic			
	Water	Interface	Solid	Form Cluster	Water	Interface	Oil	Solid	Water	Oil	Solid	Form Cluster
20	13	1	5	0	10	2	5	3	4	15	1	2
40	13	0	6	0	8	3	5	4	2	18	0	2
60	16	0	4	0	8	1	9	2	1	19	0	3
80	16	1	3	0	6	5	7	2	1	18	1	4
100	14	0	6	0	5	4	8	3	1	18	1	5
120	15	0	5	1	6	4	8	2	1	17	2	4
140	14	0	6	1	8	4	8	0	0	17	2	5
160	14	0	6	1	6	4	7	3	0	18	2	5
180	15	0	5	1	5	6	5	4	0	19	1	5
200	13	0	7	1	5	5	7	3	0	20	0	5

The micro-behaviors of the NPs underlie the diffusion dynamics of the NPs, thus their mean square displacement (MSD), and the stability of their relative positions in the nanochannels. As shown by the MSD of NPs in equilibrium shown in Fig. 3(a) (the last 1 ns of the long equilibration), the mixed NPs have the highest mobility while the hydrophobic ones have the lowest. The stability of the NPs distribution in the nanochannels can be characterized by the root-mean-square deviation (RMSD) of the relative positions of the NPs, as shown in Fig. 3(b). Specifically, the hydrophobic NPs reach a stable distribution after 100 ns, as the corresponding RMSD shows a plateau (black curve, Fig. 3(b)). Although the RMSD of the hydrophilic and the mixed feature a slow increasing pattern in the second half of the equilibration (from 100 ns to 200 ns), meaning only slight changes in the relative positions of the NPs, some individual NPs are found to dwell at specific positions in the nanochannel. As MSD of each NP shown in Fig. 3(c–e), some NPs seem stuck at positions with significant dwelling time spans (flat portion of the MSD curves). The stuck NPs indicate strong atomistic adhering force at the corresponding positions in the nanochannels, also the alteration of the local pressure especially those trapped stably at the oil-water interface and the three-phase contact area, which are characterized in the following sections.

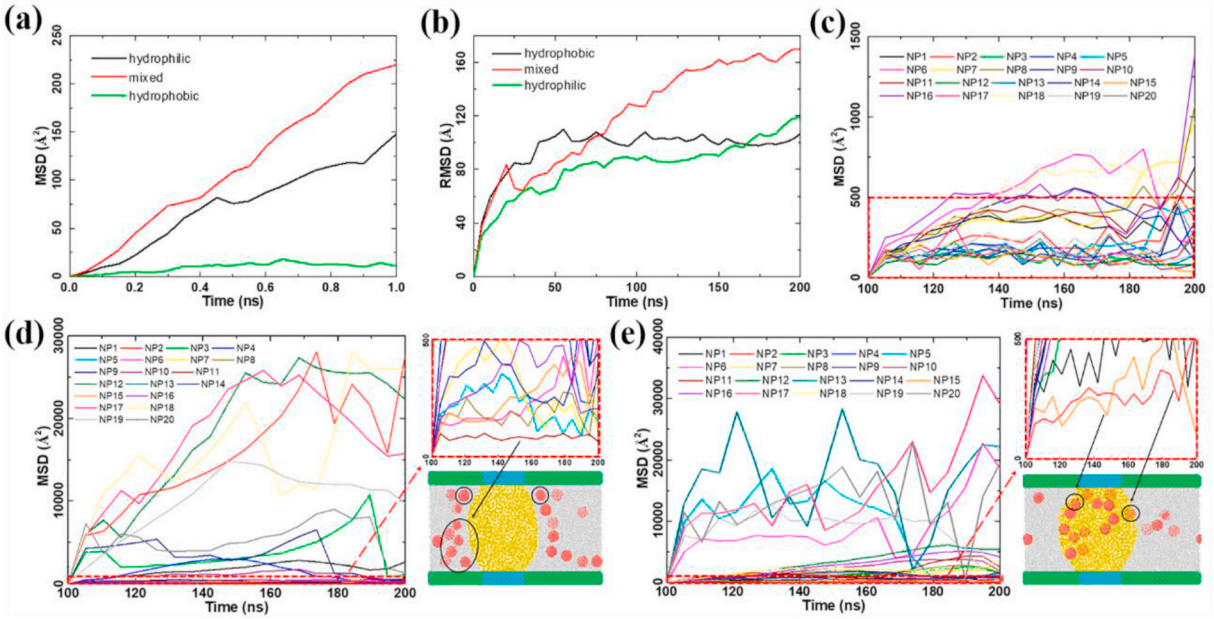

Fig. 3. (a) The MSD of different NPs in the last state of equilibration. (b) The RMSD of different NPs positions in the nanochannels in the equilibration simulations. (c) The MSD of each hydrophobic NP in the second half of the equilibration simulation. (d) The MSD of each mixed NP in equilibrium. The graph in the upper-right corner is an enlarged view of the dotted line region. The figure in the lower-right corner is one snapshot of the system, in which the NPs in a relatively stable state are marked by the black circles. (e) The MSD of each hydrophilic NP in equilibrium, with the same details in (d).

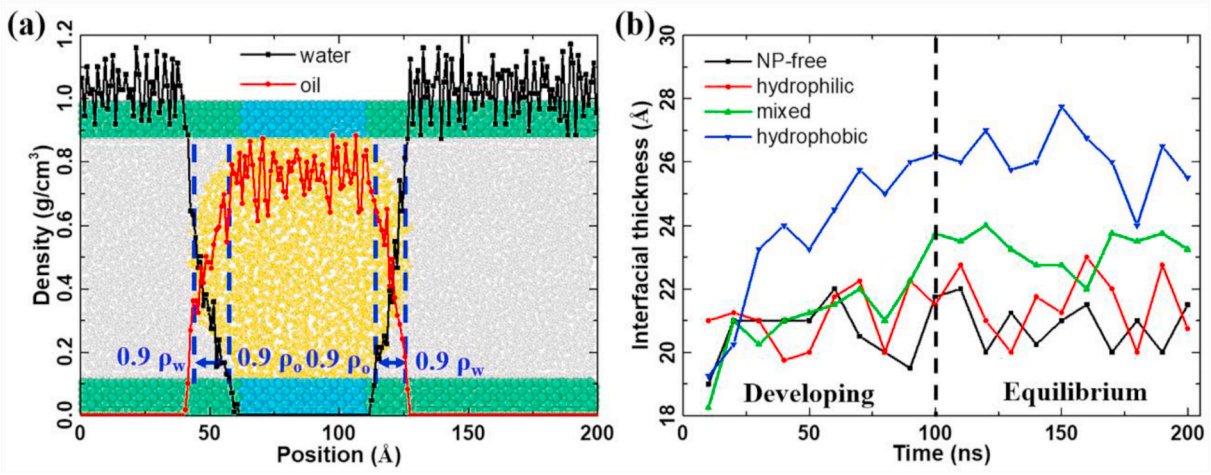

Fig. 4. (a) The density profiles in NP-free system. The oil-water interfacial thickness is defined by the distance between the two positions where the density of water and oil has 90% of the bulk value. The quantification of the interfacial thickness is exemplified in the figure by blue dash lines in the system snapshot of the base system at 5ns in the equilibration simulations. The sum of the two-interval distances is the interfacial thickness. The density profiles of water and oil along the nanochannel are shown in black and red respectively in the figure (b) Interfacial thickness evolution in the 4 system in equilibration. The black dash line at 100 ns simulation time separates two stages of the interfacial thickness profiles. (For interpretation of the references to colour in this figure legend, the reader is referred to the Web version of this article.)

High local pressure locations in the nanochannel in the systems with NPs correspond to the positions of the NPs, and the higher concentration of NPs the higher local pressure (Müller et al., 2004; Tanvir and Qiao, 2012). Specifically, high local pressure appears in the oil phase for the system with hydrophobic NPs. In contrast, the local pressure profile shows a concave pattern in the system with hydrophilic NPs, with high pressure observed close to the oil-water interfaces at both sides of the oil droplet. The local pressure distribution is more even along the nanochannel in the system with mixed NPs, where apex pressure values are also found close to the oil-water interface. Given the positions of the nanoparticles in the confined nanochannel exhibited small fluctuations in equilibration, longer sampling windows of continual 5-ns equilibration trajectories are used to further confirm the average results obtained by the non-continual small sampling windows shown in Fig. 5 (a). The calculated local pressure profiles from the average of the whole 5-ns trajectories yield the same results (Fig. 5(b)).

From the atomistic point of view, high local pressure indicates the great binding affinity of small molecules to NPs. Thus, the NPs with the surrounding oil/water molecules have a high possibility to diffuse in a cluster. Hydrophobic NPs are more likely to disturb the oil droplet structure from the inside of the oil droplet under external driving force. In contrast, the hydrophilic NPs introduce high local pressure close to the oil-water interface and the three-phase contact area as shown above in the micro-behaviors of NPs. The movement of the hydrophilic NPs in

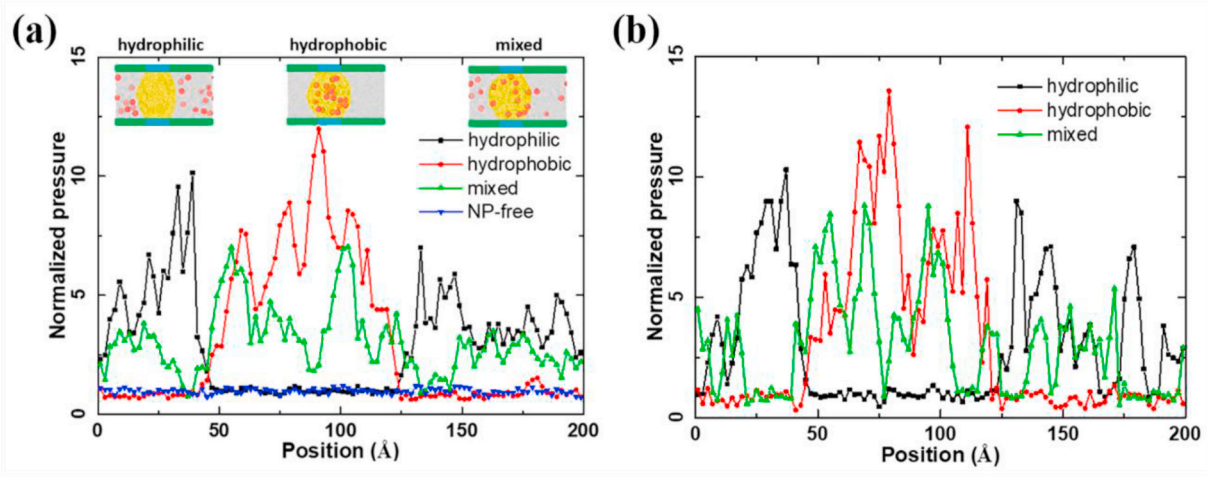

Fig. 5. (a) Comparison of local pressure profiles along the channel in the 4 systems. Local pressure obtained in the systems with NPs is normalized by the base system (NP free) for better visualization of the differences. For auxiliary observation, three representative snapshots (hydrophilic, hydrophobic, and mixed) are placed at the top. (b) The local pressure profiles calculated by averaging whole equilibration trajectories of 5 ns.

the three-phase contact area can strongly influence the displacement of the three-phase contact line of the oil droplets. The mixed NPs feature partially the effect of both the hydrophobic and hydrophilic NPs. It should be noted that high local pressure induced by the injection of NPs can contribute to possible jamming of the nanochannels and bring impacts to the fluid dynamics in the nanochannel, which is beyond the scope of this study.

3.2.2. Local pressure distribution in the three-phase contact area

NPs in the three-phase contact area are believed to be highly important to EOR (Chengara et al., 2004). Because the hydrophilic NPs in this study have a high tendency to accumulate in the three-phase contact area, the resulting local pressure deserves further investigation. Representative and independent snapshots of hydrophilic NPs in the three-phase contact area in the second half of the equilibration simulation are chosen to study the induced local pressure in that important area. As shown in Fig. 6, the highest pressure in the three-phase contact area at all times is induced by the innermost NP to the three-phase contact line. At the same time, all the pressure profiles show a tendency to decrease with distance from the three-phase contact line. The exceedingly high pressure associated with the innermost NP to the three-phase contact line indicates the strong interactions of the hydrophilic NP with its surrounding molecules, in this case, are with both oil and water molecules. Such high local pressure increases the possibility of the NP to disturb the stability of the three-phase contact line and also the whole three-phase contact area, which can alter the oil droplet displacement dynamics under external force. In other words, the hydrophilic NPs accumulated at the three-phase contact area could be beneficial to EOR, further experimental verification can be of great interest in future studies.

4. Discussion

Atomistic modeling and MD simulations provide detailed nanoscale information that is difficult to obtain in large scale flooding experiments, especially on the interactions among different components in the complex nanofluids system in the reservoir. Such knowledge is crucial to nanoparticle formulation in nano-enabled petroleum engineering. The current design of the simulation models features different distribution of NPs into nanochannels with trapped oil droplets, which supplies the possibility of comparing and revealing the characteristics of dynamics and mechanics of injected NPs in the vicinity of oil droplets. Among the NPs, the mixed NPs have the highest mobility in the nanochannel and can possibly avoid the jamming of nanoparticles in the narrow channels. Also, the mixed NPs are observed to adsorb at the interface, which can lower the interfacial tension and is beneficial for the subsequent detachment of oil droplets. The hydrophilic NPs in this study show an obvious tendency of adsorbing in the three-phase contact area and impose high local pressure, which facilitates the easier movement of the three-phase contact line. The hydrophilic NPs also can absorb onto the structured water layer on the solid, which could contribute to the wettability alteration of the nanochannel, similar to the results predicted by former studies (Xiao Wang, Xiao, Zhang and He, 2017). The hydrophobic NPs accumulating inside the oil droplet drastically increase the volume of the droplet, which also subsequently alters the thickness of the oil-water interface. The three types of NPs thus bring highly distinct changes inside the nanochannel, any possible corresponding contributing effects of which on the displacement of the trapped oil droplets thus should rely on different mechanisms. In EOR application, the modified mixed NPs which could partly aggregate in the three-phase contact area and partly adsorbed at the interface would be an ideal choice. Of course, when the flooding force provided is large enough, the hydrophobic NPs can also effectively disperse trapped oil droplets with the large interactions.

The local pressure in the three-phase contact area for NP-free system does not show any extraordinarily high value, as shown in Fig. 7(a). With the injection and accumulation of hydrophilic NPs, the local pressure in the three-phase contact area exhibits remarkably high value, which closely resembles the so-called structural disjoining pressure monitored in previous studies (Fig. 7(b)) (Wasan and Nikolov, 2003). The analytical formulation of the structural disjoining pressure theory assumes the oil phase and the substrate as the continuum medium that sandwich the nanoparticles in the three-phase contact area. This study disregards such assumption but treats the oil/water molecules explicitly. From such atomistic scope, the water molecules near the three-phase contact line have strong interactions with the surface of hydrophilic NPs and at the same time experience confinement effects from repellence of the oil molecules. The water molecules near the innermost nanoparticles suffer the greatest space confinement effect, which ultimately leads to the high local pressure value near the innermost nanoparticle and the pressure gradient in the three-phase contact area. Although the structural disjoining pressure has been utilized in explaining many experiments, the current results provide for the first-time further support from the atomistic level, and thus deepen the understanding of the theoretical fundamentals of EOR. Despite the displacement of the oil droplet is not the focus of this study, the high

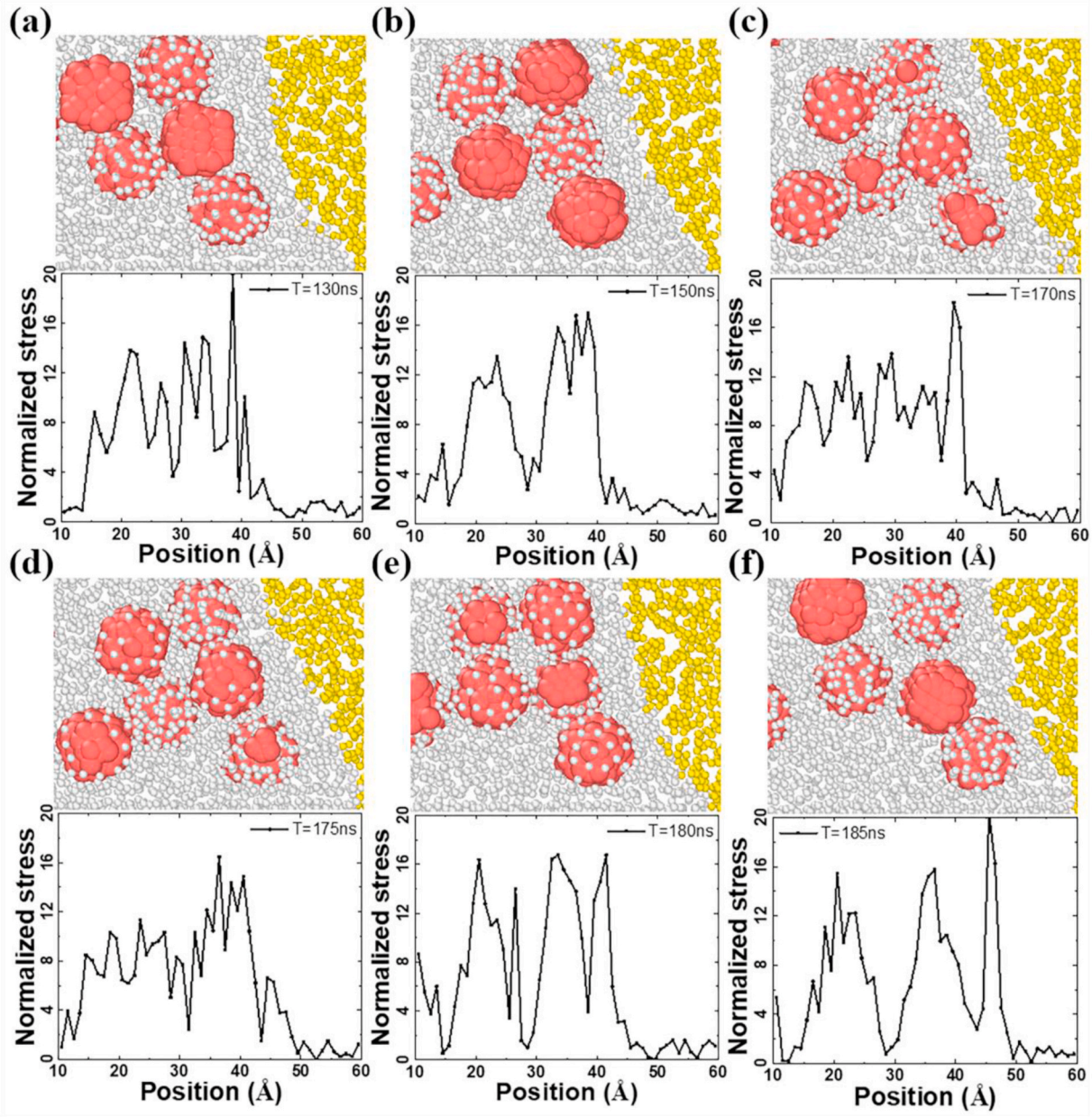

Fig. 6. Local pressure in the three-phase contact area induced by hydrophilic NPs. (a–f) Local pressure monitored at the three-phase contact area at different times. All the pressure profiles are normalized by the pressure monitored at the same position in the base system. The corresponding snapshots of NPs in the three-phase contact area are given in each figure. The x-axis in each figure indicates the location of the upper snapshot in the nanochannel.

local pressure induced by the innermost of NP to the three-phase contact line and the decrease pattern of local pressure in the three-phase contact area should have the same function as the structural disjoining pressure. The local pressure profiles found in the system with hydrophilic NPs apply to trapped oil droplets not only with a large contact angle of the oil phase but also with a large contact angle of the water phase. Like the system shown in Fig. 7(c) for comparison, hydrophilic NPs also prefer to stay stably in the three-phase contact area and trigger similar local pressure distribution in the area.

Based on the results that hydrophilic NPs can accumulate in the three-phase contact area and hydrophobic NPs can enlarge the interface thickness, there could be an interesting synergistic effect if a mixture of the two NPs were used together. With the mixture of hydrophobic and hydrophilic NPs appearing in the trapped oil droplet system in nanochannels in reservoirs, the enlarged width of the oil-water interface by hydrophobic NPs could enlarge the three-phase contact region. With that, more hydrophilic NPs could potentially aggregate in the three-phase contact region and result in higher structural disjoining pressure. The potential of such a possible synergistic effect in EOR is subjected to further investigation in the future step of this work.

It should be noted that the trapped oil droplet is one primitive representation of the real cases in the oil reservoir. In future work, the role of NPs in nanochannel systems with other types of remaining oil needs to be studied, which can provide a more complete view on nanofluids for EOR and enable better design and optimization of NPs for recovery of specified types of the remaining oil. The nanoparticles modeled in this work maintain stably in their structure and properties throughout the simulations, which cannot cover the interesting phenomena associated with changes in nanoparticles. In addition, clarifying the relationship between structural disjoining pressure and wettability alteration can be of interest.

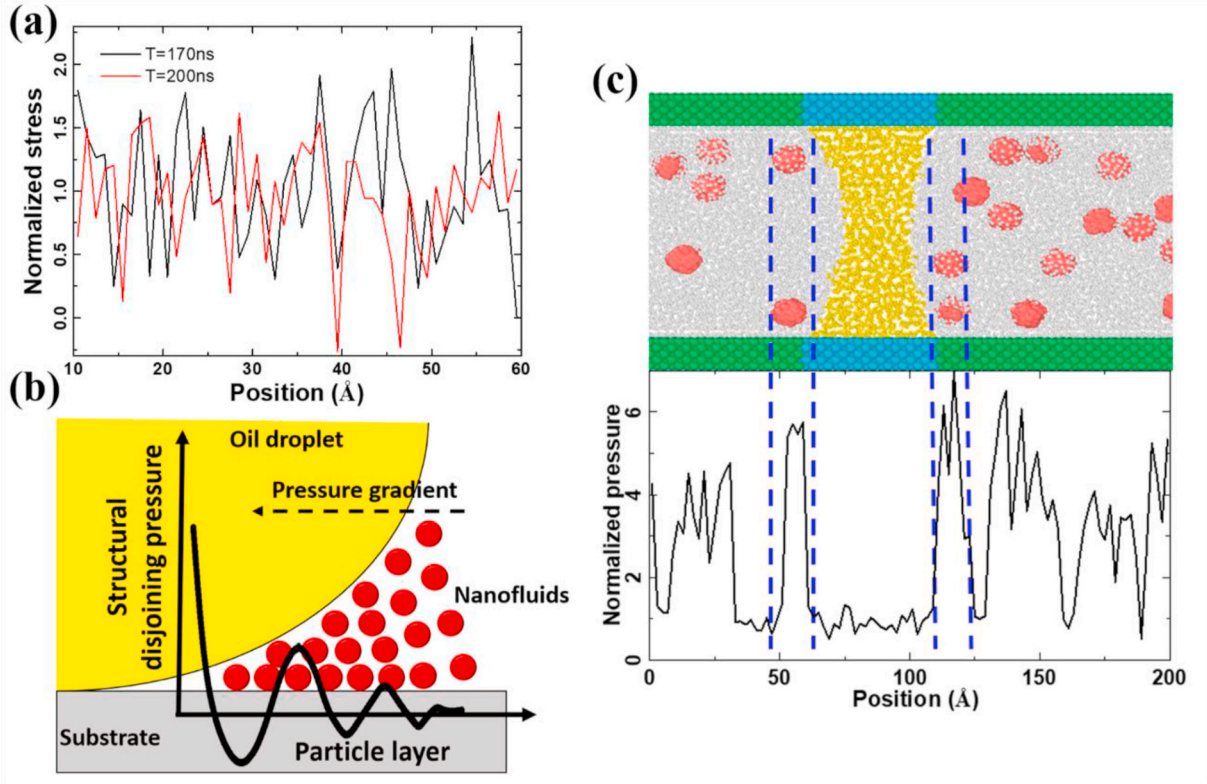

Fig. 7. (a) Local pressure in the three-phase contact area at different simulation times in the NP-free system. (b) Schematic presentation of structural disjoining pressure induced by the aggregation of nanoparticles in the three-phase contact area. (c) Hydrophilic NPs dwelling in the three-phase contact area of a trapped oil droplet with a large contact angle of the water phase. The system shares the same modeling and simulation parameters with other systems. The snapshot is taken at 200 ns of the equilibration simulation. The pressure profile in the three-phase contact area is marked with the corresponding NPs.

5. Conclusions

The trapped oil droplet/nanofluid systems in the confined channel have been studied by atomistic modeling and MD simulations. The results indicate that the distribution of NPs in the nanochannels and the resulting local pressure profiles are dominated by the wettability of NPs. Hydrophobic NPs are prone to enter the oil droplet as clusters, which leads to increasing interfacial thickness and high pressure inside the oil droplet. Mixed NPs have the highest mobility in both the oil and water phases in the nanochannel, and favor dwelling at the oil-water interface. The local pressure distribution induced by mixed NPs is relatively uniform along the channel, with the higher surrounding the oil droplet. Hydrophilic NPs can only disperse in water and are prone to adsorb in the three-phase contact areas. High local pressure can be induced by hydrophilic NPs aggregating near the oil-water interfaces. Importantly, the local pressure raised by hydrophilic NPs in the three-phase contact region is reminiscent of formerly reported structural disjoining pressure, which supports the mechanism of structural disjoining pressure for the first time from the perspective of atomistic modeling. In summary, the study provides atomistic insight into trapped oil/nanofluid in a confined channel system, which is hardly investigated by the relevant experiments. The results elucidate the effects of varied NPs in altering the local pressure in oil trapping nanochannels, which deepens the nano-mechanical fundamentals of petroleum science and engineering. Furthermore, the finding can be adopted in the design and screen of NPs for EOR and nanofluid applications in other fields. Last but not least, this study paves an avenue for future studies on the controlling factors of structural disjoining pressure and the mechanism of NPs on other important types of residual oil at the nanoscale.

Credit author statement

Yuanhao Chang: Conceptualization, Writing – original draft. Senbo Xiao: Methodology, Software. Yuequn Fu: Investigation. Xiao Wang: Resources, Investigation. Zhiliang Zhang: Supervision. Jianying He: Validation, Writing – review & editing.

Declaration of competing interest

The authors declare that they have no known competing financial interests or personal relationships that could have appeared to influence the work reported in this paper.

Acknowledgments

This work was financially supported by the Research Council of Norway (Grant No. 234626) and the Chinese Scholarship Council. The supercomputer CPU hours were provided by the Norwegian Metacenter for Computational science (Project ID: NN9110K and NN9391K).

References

Abidin, A., Puspasari, T., Nugroho, W., 2012. Polymers for enhanced oil recovery technology. Procedia Chemistry 4, 11–16.
Al-Anssari, S., Barifcani, A., Wang, S., Maxim, L., Iglauer, S., 2016. Wettability alteration of oil-wet carbonate by silica nanofluid. J. Colloid Interface Sci. 461, 435–442.
Atomic, L.-s., Simulator, M.M.P., 2003. LAMMPS Users Manual.
Bera, A., Belhaj, H., 2016. Application of nanotechnology by means of nanoparticles and nanodispersions in oil recovery-A comprehensive review. J. Nat. Gas Sci. Eng. 34, 1284–1309.
Chengara, A., Nikolov, A.D., Wasan, D.T., Trokhymchuk, A., Henderson, D., 2004. Spreading of nanofluids driven by the structural disjoining pressure gradient. J. Colloid Interface Sci. 280 (1), 192–201.

Dai, C., Wang, X., Li, Y., Lv, W., Zou, C., Gao, M., Zhao, M., 2017. Spontaneous imbibition investigation of self-dispersing silica nanofluids for enhanced oil recovery in low-permeability cores. Energy Fuel. 31 (3), 2663–2668.
Dehghan Monfared, A., Ghazanfari, M.H., Jamialahmadi, M., Helalizadeh, A., 2016. Potential application of silica nanoparticles for wettability alteration of oil–wet calcite: a mechanistic study. Energy Fuel. 30 (5), 3947–3961.
Douillard, J.M., 2009. Experimental approach of the relation between surface tension and interfacial thickness of simple liquids. J. Colloid Interface Sci. 337 (1), 307–310.
Frost, D.S., Dai, L.L., 2012. Molecular dynamics simulations of charged nanoparticle self-assembly at ionic liquid-water and ionic liquid-oil interfaces. J. Chem. Phys. 136 (8), 084706.
Giraldo, J., Benjumea, P., Lopera, S., Cortés, F.B., Ruiz, M.A., 2013. Wettability alteration of sandstone cores by alumina-based nanofluids. Energy Fuel. 27 (7), 3659–3665.
Hendraningrat, L., Li, S., Torsæter, O., 2013. A coreflood investigation of nanofluid enhanced oil recovery. J. Petrol. Sci. Eng. 111, 128–138.
Hendraningrat, L., Torsæter, O., 2016. A study of water chemistry extends the benefits of using silica-based nanoparticles on enhanced oil recovery. Appl. Nanosci. 6 (1), 83–95.
Hoover, W.G., 1985. Canonical dynamics: equilibrium phase-space distributions. Phys. Rev. 31 (3), 1695.
Hu, Z., Azmi, S.M., Raza, G., Glover, P.W., Wen, D., 2016. Nanoparticle-assisted water-flooding in Berea sandstones. Energy Fuel. 30 (4), 2791–2804.
Jha, N.K., Lebedev, M., Iglauer, S., Ali, M., Roshan, H., Barifcani, A., Sarmadivaleh, M., 2020. Pore scale investigation of low salinity surfactant nanofluid injection into oil saturated sandstone via X-ray micro-tomography. J. Colloid Interface Sci. 562, 370–380.
Keykhosravi, A., Simjoo, M., 2019. Insights into stability of silica nanofluids in brine solution coupled with rock wettability alteration: an enhanced oil recovery study in oil-wet carbonates. Colloid. Surface. Physicochem. Eng. Aspect. 583, 124008.
Khedr, A., Striolo, A., 2020. Self-assembly of mono- and poly-dispersed nanoparticles on emulsion droplets: antagonistic vs. synergistic effects as a function of particle size. Phys. Chem. Chem. Phys. 22 (39), 22662–22673. https://doi.org/10.1039/d0cp02588g.
Kondiparty, K., Nikolov, A.D., Wasan, D., Liu, K.L., 2012. Dynamic spreading of nanofluids on solids. Part I: experimental. Langmuir 28 (41), 14618–14623. https://doi.org/10.1021/la3027013.
Kuang, W., Saraji, S., Piri, M., 2018. A systematic experimental investigation on the synergistic effects of aqueous nanofluids on interfacial properties and their implications for enhanced oil recovery. Fuel 220, 849–870.
Lake, L.W., Johns, R., Rossen, W.R., Pope, G.A., 2014. Fundamentals of enhanced oil recovery.
Leroy, F., 2016. Revisiting the droplet simulation approach to derive force-field parameters for water on molybdenum disulfide from wetting angle measurements. J. Chem. Phys. 145 (16), 164705.
Li, S., Torsæter, O., 2015. Experimental investigation of the influence of nanoparticles adsorption and transport on wettability alteration for oil wet berea sandstone. Paper presented at the SPE Middle East Oil & Gas Show and Conference.
Lim, S., Horiuchi, H., Nikolov, A.D., Wasan, D., 2015. Nanofluids alter the surface wettability of solids. Langmuir 31 (21), 5827–5835.
Liu, K.L., Kondiparty, K., Nikolov, A.D., Wasan, D., 2012. Dynamic spreading of nanofluids on solids part II: modeling. Langmuir 28 (47), 16274–16284. https://doi.org/10.1021/la302702g.
Luu, X.C., Yu, J., Striolo, A., 2013a. Ellipsoidal Janus nanoparticles adsorbed at the water-oil interface: some evidence of emergent behavior. J. Phys. Chem. B 117 (44), 13922–13929. https://doi.org/10.1021/jp407495z.
Luu, X.C., Yu, J., Striolo, A., 2013b. Nanoparticles adsorbed at the water/oil interface: coverage and composition effects on structure and diffusion. Langmuir 29 (24), 7221–7228. https://doi.org/10.1021/la304828u.
Martin, M.G., Siepmann, J.I., 1998. Transferable potentials for phase equilibria. 1. United-atom description of n-alkanes. J. Phys. Chem. B 102 (14), 2569–2577.
Matar, O., Craster, R., Sefiane, K., 2007. Dynamic spreading of droplets containing nanoparticles. *Physical Review E, 76*(5), 056315.
Metin, C.O., Baran, J.R., Nguyen, Q.P., 2012. Adsorption of surface functionalized silica nanoparticles onto mineral surfaces and decane/water interface. J. Nanoparticle Res. 14 (11), 1246.
Mohanraj, V., Chen, Y., 2006. Nanoparticles-a review. Trop. J. Pharmaceut. Res. 5 (1), 561–573.
Molinero, V., Moore, E.B., 2009. Water modeled as an intermediate element between carbon and silicon. J. Phys. Chem. B 113 (13), 4008–4016.
Müller, F., Peukert, W., Polke, R., Stenger, F., 2004. Dispersing nanoparticles in liquids. Int. J. Miner. Process. 74, S31–S41.
Nazari Moghaddam, R., Bahramian, A., Fakhroueian, Z., Karimi, A., Arya, S., 2015. Comparative study of using nanoparticles for enhanced oil recovery: wettability alteration of carbonate rocks. Energy Fuel. 29 (4), 2111–2119.
Ni, X., Jiang, G., Liu, F., Deng, Z., 2018. Synthesis of an amphiphobic nanofluid with a novel structure and its wettability alteration on low-permeability sandstone reservoirs. Energy Fuel. 32 (4), 4747–4753.
Nicot, B., Jafari Daghlian Sofla, S., Anne James, L., Zhang, Y., 2019. Toward a mechanistic understanding of wettability alteration in reservoir rocks using silica nanoparticles. E3S Web of Conferences 89. https://doi.org/10.1051/e3sconf/20198903004.
Nosé, S., 1984. A unified formulation of the constant temperature molecular dynamics methods. J. Chem. Phys. 81 (1), 511–519.
Plimpton, S., 1993. Fast Parallel Algorithms for Short-Range Molecular Dynamics (Retrieved from).
Plimpton, S., Crozier, P., Thompson, A., 2007. LAMMPS-large-scale atomic/molecular massively parallel simulator. Sandia National Laboratories 18, 43.
Rafiee, J., Mi, X., Gullapalli, H., Thomas, A.V., Yavari, F., Shi, Y., Koratkar, N.A., 2012. Wetting transparency of graphene. Nat. Mater. 11 (3), 217–222.
Rahimi, K., Adibifard, M., 2015. Experimental study of the nanoparticles effect on surfactant absorption and oil recovery in one of the Iranian oil reservoirs. Petrol. Sci. Technol. 33 (1), 79–85.
Ravera, F., Santini, E., Loglio, G., Ferrari, M., Liggieri, L., 2006. Effect of nanoparticles on the interfacial properties of liquid/liquid and liquid/air surface layers. J. Phys. Chem. B 110 (39), 19543–19551.
Rezk, M.Y., Allam, N.K., 2019. Unveiling the synergistic effect of ZnO nanoparticles and surfactant colloids for enhanced oil recovery. Colloid and Interface Science Communications 29, 33–39.
Rostami, P., Sharifi, M., Aminshahidy, B., Fahimpour, J., 2019. Enhanced oil recovery using silica nanoparticles in the presence of salts for wettability alteration. J. Dispersion Sci. Technol.
Sedghi, M., Piri, M., Goual, L., 2016. Atomistic molecular dynamics simulations of crude oil/brine displacement in calcite mesopores. Langmuir 32 (14), 3375–3384.
Shah, A., Fishwick, R., Wood, J., Leeke, G., Rigby, S., Greaves, M., 2010. A review of novel techniques for heavy oil and bitumen extraction and upgrading. Energy Environ. Sci. 3 (6), 700–714.
Sonne, J., Hansen, F.Y., Peters, G.H., 2005. Methodological problems in pressure profile calculations for lipid bilayers. J. Chem. Phys. 122 (12), 124903.
Sumer, Z., Striolo, A., 2020. Nanoparticles shape-specific emergent behaviour on liquid crystal droplets. Molecular Systems Design & Engineering 5 (2), 449–460. https://doi.org/10.1039/c9me00153k.
Tanvir, S., Qiao, L., 2012. Surface tension of nanofluid-type fuels containing suspended nanomaterials. Nanoscale research letters 7 (1), 1–10.
Wang, X., Xiao, S., Zhang, Z., He, J., 2017. Effect of nanoparticles on spontaneous imbibition of water into ultraconfined reservoir capillary by molecular dynamics simulation. Energies 10 (4), 506.
Wang, X., Xiao, S., Zhang, Z., He, J., 2018a. Displacement of nanofluids in silica nanopores: influenced by wettability of nanoparticles and oil components. Environ. Sci.: Nano 5 (11), 2641–2650.
Wang, X., Xiao, S., Zhang, Z., He, J., 2019. Transportation of Janus nanoparticles in confined nanochannels: a molecular dynamics simulation. Environ. Sci.: Nano 6 (9), 2810–2819. https://doi.org/10.1039/c9en00314b.
Wang, X., Zhang, Z., Torsaeter, O., He, J., 2018b. Atomistic insights into the nanofluid transport through an ultra-confined capillary. Phys. Chem. Chem. Phys. 20 (7), 4831–4839. https://doi.org/10.1039/c7cp08140e.
Wasan, D.T., Nikolov, A.D., 2003. Spreading of nanofluids on solids. Nature 423 (6936), 156–159.
Wu, H., Chen, J., Liu, H., 2015. Molecular dynamics simulations about adsorption and displacement of methane in carbon nanochannels. J. Phys. Chem. C 119 (24), 13652–13657.
Xu, J., Zhang, Y., Chen, H., Wang, P., Xie, Z., Yao, Y., Zhang, J., 2013. Effect of surfactant headgroups on the oil/water interface: an interfacial tension measurement and simulation study. J. Mol. Struct. 1052, 50–56.
Yesudasan, S., 2019. Thin film pressure estimation of argon and water using LAMMPS. Int. J. Eng. 12 (1), 1.
Youssif, M.I., El-Maghraby, R.M., Saleh, S.M., Elgibaly, A., 2018. Silica nanofluid flooding for enhanced oil recovery in sandstone rocks. Egyptian Journal of Petroleum 27 (1), 105–110.
Zhang, H., Nikolov, A., Wasan, D., 2014. Enhanced oil recovery (EOR) using nanoparticle dispersions: underlying mechanism and imbibition experiments. Energy Fuel. 28 (5), 3002–3009.